

Article

The Effect of Nitrogen Incorporation on the Optical Properties of Si-Rich a-SiC_x Films Deposited by VHF PECVD

Hongliang Li, Zewen Lin ^{*}, Yanqing Guo, Jie Song, Rui Huang and Zhenxu Lin

School of Materials Science and Engineering, Hanshan Normal University, Chaozhou 521041, China; lihl4@hstc.edu.cn (H.L.); yqguo126@126.com (Y.G.); songjie@hstc.edu.cn (J.S.); rhuang@hstc.edu.cn (R.H.); lzx2016@hstc.edu.cn (Z.L.)

* Correspondence: zewenlin@126.com

Abstract: The influence of N incorporation on the optical properties of Si-rich a-SiC_x films deposited by very high-frequency plasma-enhanced chemical vapor deposition (VHF PECVD) was investigated. The increase in N content in the films was found to cause a remarkable enhancement in photoluminescence (PL). Relative to the sample without N incorporation, the sample incorporated with 33% N showed a 22-fold improvement in PL. As the N content increased, the PL band gradually blueshifted from the near-infrared to the blue region, and the optical bandgap increased from 2.3 eV to 5.0 eV. The enhancement of PL was suggested mainly from the effective passivation of N to the nonradiative recombination centers in the samples. Given the strong PL and wide bandgap of the N incorporated samples, they were used to further design an anti-counterfeiting label.

Keywords: photoluminescence; thin films; optical properties; SiC_x



Citation: Li, H.; Lin, Z.; Guo, Y.; Song, J.; Huang, R.; Lin, Z. The Effect of Nitrogen Incorporation on the Optical Properties of Si-Rich a-SiC_x Films Deposited by VHF PECVD. *Micromachines* **2021**, *12*, 637. <https://doi.org/10.3390/mi12060637>

Academic Editor: Hieu Pham
Trung Nguyen

Received: 26 April 2021
Accepted: 27 May 2021
Published: 30 May 2021

Publisher's Note: MDPI stays neutral with regard to jurisdictional claims in published maps and institutional affiliations.



Copyright: © 2021 by the authors. Licensee MDPI, Basel, Switzerland. This article is an open access article distributed under the terms and conditions of the Creative Commons Attribution (CC BY) license (<https://creativecommons.org/licenses/by/4.0/>).

1. Introduction

The motivation to realize monolithic optoelectronic integrated circuits has spurred great efforts to explore efficient Si-based light sources that can operate at room temperature and is compatible with the mainstream complementary metal-oxide-semiconductor technology (Fadaly, Dijkstra et al. 2020) [1–6]. Thus far, different techniques such as plasma-enhanced chemical vapor deposition and sputtering associated with appropriate post-annealing processing are being employed to obtain efficient light emission from Si-based materials [7–16]. Among the investigated materials, SiO_x and SiN_x systems have been reported to exhibit intense light emission [15,16]. However, the wide bandgap of silicon oxide (~8.5 eV) hinders the effective injection of carriers, and the material is thus unsuitable for the fabrication of stable and efficient electroluminescent devices. Meanwhile, a large number of nonradiative recombination centers in silicon nitride systems increase the difficulty of obtaining efficient electroluminescence [17]. In recent years, amorphous silicon carbide (a-SiC_x) films have also attracted much attention because of their low-cost preparation and superior physical and chemical properties, such as strong photoluminescence (PL), high doping efficiency, visible region transparency, and immense potential in the fields of Si-based photoelectric integration, photovoltaic cells, and detectors [18,19]. Thus far, a large number of studies have explored the structural, electrical, and optical properties of a-SiC_x films [20]. The experimental results have shown that the properties of a-SiC_x films are closely related to their contents of C and Si atoms and the bonding configuration between atoms. For example, the valence band edges and conduction band edges of a-SiC_x films are contributed by Si and C atoms. An increase in C content in a-SiC_x films is conducive to replacing Si–Si bonds, thereby increasing the density of silicon–carbon bonds and thus effectively widening the bandgaps of the films. The incorporation of different atoms into the materials from the working gas is a well-known process affecting the structure and physical properties of the materials [21–24]. In the previous work of our research group, by incorporating O atoms into a-SiC_x films from the oxygen gas flow

with PECVD technique, the influence of O doping on the luminescence characteristics of a-SiC_x films was studied, and a three-level model based on the luminescence center of a Si dangling bond was established [25]. The net gain coefficient of the film was observed under ultraviolet pumping. Although efficient PL from SiC-based materials has been investigated, progress is slow. This lag is partly due to the lack of information available to correlate PL with other influence factors.

In this study, we showed the influence of N incorporation on the optical properties of Si-rich a-SiC_x films. PL measurements combined with X-ray photoelectron spectroscopy (XPS) analysis revealed that an increase in N content resulted in a remarkable enhancement in PL and switched the emitted light from the red region to the blue region. The intense tunable light emission was discussed herein. Given the strong PL and wide bandgap of N incorporated samples, they were used to design an anti-counterfeiting label in this work.

2. Experimental Details

Amorphous Si-rich a-SiC_x films with a thickness of 300 nm were fabricated by very high-frequency plasma-enhanced chemical vapor deposition (VHF PECVD, Shenyang New Blue Sky Vacuum Technology Co., Ltd., Shenyang, China) technology at a substrate temperature of 250 °C; SiH₄ and CH₄ were used as reaction gas sources. The flow rates of SiH₄ and CH₄ were set at 2.5 and 5 sccm, respectively. During the preparation phase, the flow rates of NH₃ were introduced and set as 0, 5, 10, and 15 sccm to investigate the effects of N incorporation on a-SiC_x. The room temperature PL and PL decay characteristics of the films were measured with an Edinburgh FLS1000 fluorescence spectrometer. The absorption spectra of the films were obtained with a Shimadzu UV-3600 spectrophotometer. The microstructures of the films were evaluated using the Horiba LabRAM HR Evolution Raman spectrometer. The Si, C, and N contents in the films were determined by XPS (Thermo-VG Scientific ESCALAB 250, Waltham, MA, USA). The bonding structures were examined by a Fourier transform infrared (FTIR) spectrometer.

3. Results and Discussion

Figure 1 shows the Si, N, and C contents of the films prepared with different NH₃ flow rates. When the NH₃ flow rate was zero, the Si and C contents of the films were 71% and 29%, respectively. These values indicated that the films were Si-rich silicon carbides. As the NH₃ flow rate increased from 5 sccm to 15 sccm, the film composition changed significantly. When the NH₃ flow rate was 5 sccm, the Si and C contents of the films remarkably decreased to 53% and 14%, respectively, while the N content rapidly increased to 33%. As the NH₃ flow increased further, the Si and C contents of the films decreased continuously while the N content increased.

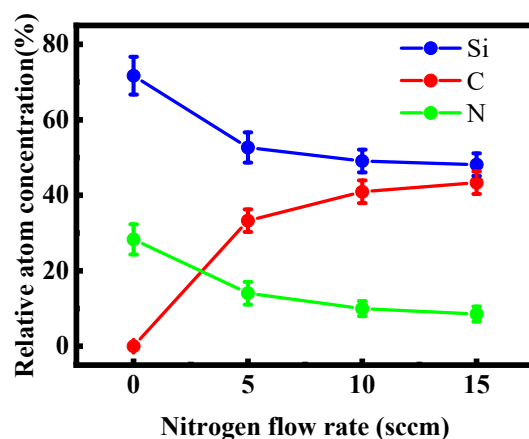


Figure 1. Si, N, and C contents of the samples fabricated at different NH₃ flow rates.

Figure 2 presents the Raman scattering spectra of the films with different N contents. A dominant Raman peak appeared at around 480 cm^{-1} , which was attributed to the transverse optical vibration mode of the amorphous silicon [26]. A weak peak at $\sim 790\text{ cm}^{-1}$ corresponded to the longitudinal optical vibration mode of SiC [26]. The results indicated that Si–Si and Si–C bonds existed in the form of an amorphous structure and no other Si and/or SiC nanocrystalline structure was produced in the films.

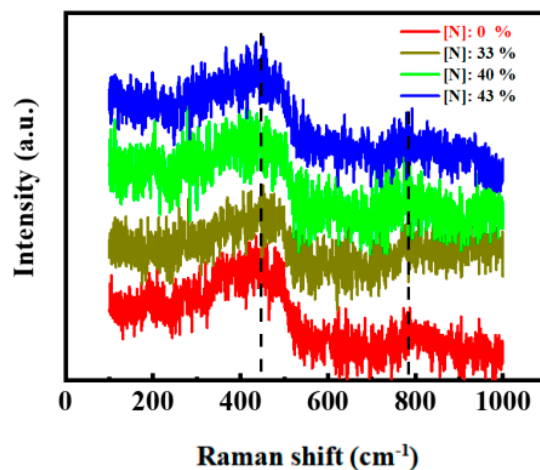


Figure 2. Raman spectrum of the films with different N content.

The FTIR spectrometer was employed to clarify the bonding configurations of the films incorporated with different N contents, and the results are shown in Figure 3. The absorption peak at $\sim 640\text{ cm}^{-1}$ corresponded to the SiH_n rocking vibration [27]. The absorption peak at $\sim 780\text{ cm}^{-1}$ corresponded to the Si–C stretching vibration [23]. The $\sim 850\text{ cm}^{-1}$ absorption peak was ascribed to the Si–N stretching vibration [28]. The absorption band at $\sim 1000\text{ cm}^{-1}$ was associated with the Si–CH₂ stretching vibration, and the 1250 cm^{-1} absorption peak was ascribed to the C–H_n stretching vibration [27]. The peak at $\sim 2140\text{ cm}^{-1}$ bands was connected to the Si–H stretching mode [27]. The 3350 cm^{-1} peak corresponded to the N–H stretching mode [28]. As shown in Figure 3, the SiH_n rocking vibration disappeared while the Si–C and Si–N stretching vibrations strengthened as the N content increased in the films. Therefore, the films mainly existed in the form of Si–C and Si–N bond structures.

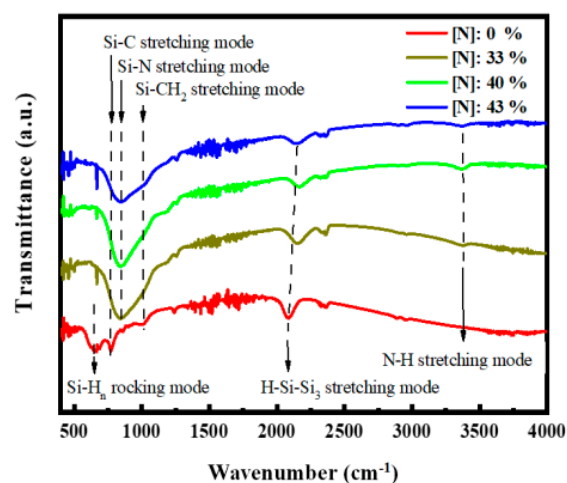


Figure 3. FTIR absorption spectra of the samples with different N contents.

Figure 4 shows the transmission spectra of the films with different N contents. With the increase in the N content from 0% to 43%, the absorption edge moved toward the

short-wave direction, indicating that the increase in the N content effectively widened the optical bandgap of the films. According to the formula [29]:

$$ad = -\ln T \quad (1)$$

where T is the transmittance and d is the film thickness. The absorption coefficient a of the film can be obtained, as shown in the inset of Figure 4. In our case, the optical bandgap E_{04} was defined as the photon energy corresponding to the absorption coefficient $\alpha = 10^4 \text{ cm}^{-1}$ [29]. As indicated in the inset of Figure 4, the increase in the N content from 0% to 43% resulted in a notable increase in the optical bandgap E_{04} from 2.3 eV to 5.0 eV. Our experimental results indicated that N plays an important role in the modulation of the optical bandgap of Si-rich SiCx.

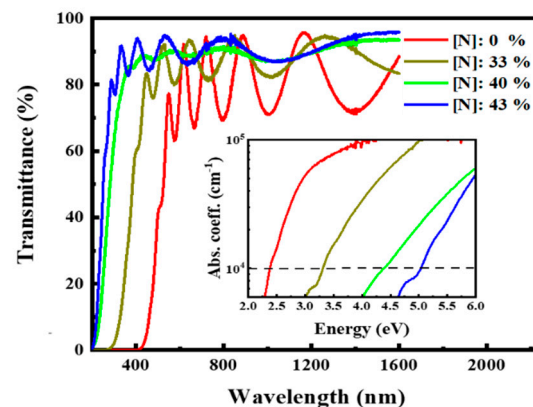


Figure 4. Transmission spectra of the samples with different N contents. Inset shows the corresponding absorption spectra.

Figure 5a displays the normalized PL spectra of the films incorporated with different N contents. For the films without N, the PL spectra, excited by the 325 nm line from the Xe lamp, peaked at around 800 nm. With the increase in N content from 0% to 43%, the PL peak blueshifted and gradually moved from ~800 nm to ~450 nm. All the films exhibited a strong visible light emission under 325 nm excitation that could be clearly observed by the naked eye in a bright room environment (Figure 5a). Moreover, the PL intensity increased rapidly with the increase in N content and reached the maximum when the N content was 33%. Compared with the films without N, the samples incorporated with N showed a 22-fold increase in PL intensity (Figure 5b). These results implied that N plays an important role in the PL of a-SiCx. That is, N can modulate the PL wavelength of a-SiCx and greatly increase PL intensity. Comparing Figures 4 and 5b showed that the change of the optical bandgap with N content was optically consistent with the change of the PL peak energy with N content (Figure 6a). In addition, the energy of the optical bandgap was significantly greater than the corresponding PL peak energy. This result suggested that PL did not originate in band-to-band recombination. The PL spectra of the films excited at different excitation wavelengths were also studied herein to gain further insights into the PL characteristics. As shown in Figure 6b, the PL peak position barely changed with the excitation wavelength increasing from 275 nm to 425 nm. This behavior was consistent with that of defect-related PL, in which the peak position was independent of the excitation wavelength because of the narrow distribution of the defect-related localized state [30]. Thus, PL was considered to originate from defect-related luminescence centers.

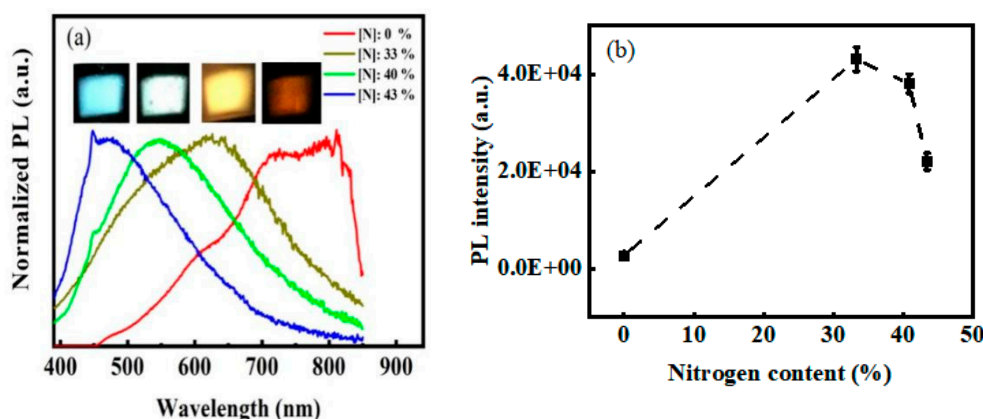


Figure 5. (a) Normalized PL spectra and (b) corresponding photoluminescence intensity of the films incorporated with different N content under an excitation wavelength of 325 nm.

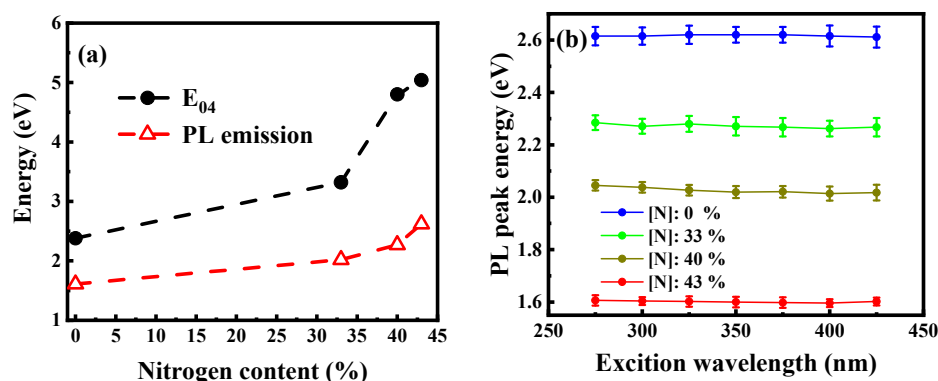


Figure 6. (a) Optical bandgap and PL peak energy of the samples as a function of N content. (b) PL peaks of the samples with different N contents as a function of excitation wavelengths.

Luminescence decay measurements were performed to further clarify the PL mechanism. Figure 7a shows the room temperature luminescence decay curves of the films. The decay curves could be well-fitted with a double exponential function. The fitted equation is as follows [31]:

$$I(t) = A_1 \exp\left(\frac{-t}{\tau_1}\right) + A_2 \exp\left(\frac{-t}{\tau_2}\right) \quad (2)$$

where I_0 is the background constant, τ_1 and τ_2 are the luminescence lifetimes of the two decay processes, and A_1 and A_2 are the proportions of the two decay processes. According to the fitting equation, the average luminescence lifetime was calculated to be in the nanosecond range, as shown in Figure 7b. This result was consistent with the defect luminescence lifetime of Si-based materials reported in the literature [16,31]. This result further supported the speculation that PL arose from defect-related luminescence centers. By comparing Figures 5b and 7b, we found that the change of the luminescence lifetime with the N content was consistent with that of the PL intensity. As shown in Figure 7b, the luminescence lifetime increased from 3.4 ns to 6.3 ns with the increase in N content from 0% to 33%. In luminescent silicon-based materials, radiative channels and nonradiative channels are involved in the recombination process of carriers. The lifetime of the nonradiative recombinations for the luminescent silicon-based materials is much shorter than that of radiative recombinations [32], and thus the increase in the measurement luminescence lifetime is mainly due to the decrease in nonradiative channels in the recombination process of carriers. Therefore, the increase in the luminescence lifetime indicated that the increase in the N content effectively passivated the nonradiative recombination centers to some extent. The Si–N bonding energy is known to be greater than the Si–Si bonding energy. Therefore, with the addition of N during the growth process, the

Si–Si bond was partially replaced by the Si–N bond. The weak Si–Si bond was particularly reduced, thereby reducing the nonradiative recombination centers. The increase in the PL intensity with the N content (Figure 5) proved this view. When the N content increased from 40% to 43%, the PL intensity gradually decreased, and the luminescence lifetime decreased from 6.2 ns to 4.2 ns. This result could be attributed to the continued increase in N that aggravated the disorder of the films and, thus, led to the increase in the nonradiative recombination centers in the films. Properly modulating the N content in Si-rich SiCx could effectively widen the optical bandgap, and an efficient light emission could be obtained.

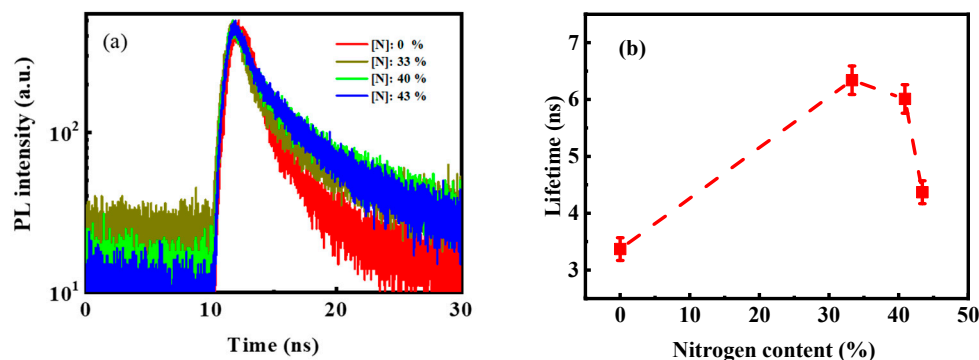


Figure 7. (a) Room-temperature luminescence decay traces and (b) lifetime taken from the samples incorporated with different N content, respectively.

On the basis of the above results, we further explored the application of N incorporation in the field of anti-counterfeiting. A film incorporated with 40% N was used to design the anti-counterfeiting symbol “T” on a quartz substrate. As shown in Figure 8a, the symbol “T” is transparent in the visible region as a result of the wide bandgap demonstrated in Figure 4. As expected, the quartz substrate exhibited a bright “T” symbol under 325 nm light irradiation because of its efficient PL properties, as shown in Figure 8b.



Figure 8. (a) The anti-counterfeiting symbol “T” on the quartz substrate. (b) The bright “T” symbol under 325 nm light irradiation.

4. Conclusions

The effects of N incorporation on the optical properties of Si-rich a-SiCx films were investigated. The increase in N content caused a significant enhancement in PL. Relative to the samples without N incorporation, those incorporated with 33% N showed a 22-fold increase in PL. Moreover, the increase in N content blueshifted the PL from the near-infrared region to the blue region and widened the optical bandgap from 2.3 eV to 5.0 eV. As indicated by the analyses of the infrared absorption spectra and PL decay characteristics, the enhancement of PL was mainly due to the effective N passivation to the nonradiative recombination centers in the samples. Given the strong PL and wide bandgap of the N incorporated samples, they were used to design an anti-counterfeiting label. Overall, the strong tunable light emission and fast decay dynamics of the films open the possibility of applying such materials to photonics and optoelectronics integration.

Author Contributions: H.L.: writing—original draft, investigation, formal analysis. Z.L. (Zewen Lin): writing—review & editing, formal analysis. Y.G.: investigation, formal analysis. J.S.: investigation. R.H.: investigation, formal analysis, writing—review & editing. Z.L. (Zhenxu Lin): formal analysis, investigation. All authors have read and agreed to the published version of the manuscript.

Funding: This work was supported by the Guangdong Basic and Applied Basic Research Foundation (2020A1515010432), Special Innovation Projects of Guangdong Provincial Department of Education (2020KTSCX076), Project of Educational Commission of Guangdong Province of China (2019KTSCX096), Young Talents in Higher Education of Guangdong (2016KQNCX100), Science and Technology Planning Projects of Chaozhou (2018GY18), and Program of the Hanshan Normal University (QN202020).

Data Availability Statement: Data underlying the results presented in this paper are not publicly available at this time but may be obtained from the authors upon reasonable request.

Conflicts of Interest: The authors declare no conflict of interest.

References

- Fadaly, E.M.T.; Dijkstra, A.; Suckert, J.R.; Ziss, D.; van Tilburg, M.A.J.; Mao, C.; Ren, Y.; van Lange, V.T.; Korzun, K.; Kölling, S.; et al. Direct-bandgap emission from hexagonal Ge and SiGe alloys. *Nature* **2020**, *580*, 205–209. [[CrossRef](#)]
- Zhang, C.; Xu, Y.; Liu, J.; Li, J.; Xiang, J.; Li, H.; Li, J.; Dai, Q.; Lan, S.; Miroshnichenko, A.E. Lighting up silicon nanoparticles with Mie resonances. *Nat. Commun.* **2018**, *9*, 2964. [[CrossRef](#)]
- Ni, Z.; Zhou, S.; Zhao, S.; Peng, W.; Yang, D.; Pi, X. Silicon nanocrystals: Unfading silicon materials for optoelectronics. *Mater. Sci. Eng. R Rep.* **2019**, *138*, 85–117. [[CrossRef](#)]
- Lin, G.R.; Wu, C.L.; Lian, C.W.; Chang, H.C. Saturated Small-Signal Gain of Si Quantum Dots Embedded in SiO₂/SiO_x/SiO₂ Strip-Loaded Waveguide Amplifier Made on Quartz. *Appl. Phys. Lett.* **2009**, *95*, 021106–021106-3. [[CrossRef](#)]
- Wang, F.; Li, N.; Jin, L.; Yang, D.; Que, D. Reduction of the efficiency droop in silicon nitride light-emitting devices by localized surface plasmons. *Appl. Phys. Lett.* **2013**, *102*, 081108. [[CrossRef](#)]
- Lin, Z.; Huang, R.; Zhang, W.; Zhang, Y.; Song, J.; Li, H.; Hou, D.; Guo, Y.; Song, C.; Wan, N.; et al. Highly Luminescent and Stable Si-Based CsPbBr₃ Quantum Dot Thin Films Prepared by Glow Discharge Plasma with Real-Time and In Situ Diagnosis. *Adv. Funct. Mater.* **2018**, *28*, 1805214–1805214-8. [[CrossRef](#)]
- Huang, R.; Song, J.; Wang, X.; Guo, Y.Q.; Song, C.; Zheng, Z.H.; Wu, X.L.; Chu, P.K. Origin of strong white electroluminescence from dense Si nanodots embedded in silicon nitride. *Opt. Lett.* **2012**, *37*, 692–694. [[CrossRef](#)] [[PubMed](#)]
- Lin, S.; Zhang, X.; Zhang, P.; Tan, D.; Xu, J.; Li, W.; Chen, K. High-efficiency near-infrared emission from Bismuth-doped SiO₂ thin films fabricated by ion implantation technology. *Opt. Lett.* **2016**, *41*, 630–633. [[CrossRef](#)]
- Kim, T.-Y.; Park, N.-M.; Kim, K.-H.; Sung, G.Y.; Ok, Y.-W.; Seong, T.-Y.; Choi, C.-J. Quantum confinement effect of silicon nanocrystals in situ grown in silicon nitride films. *Appl. Phys. Lett.* **2004**, *85*, 5355–5357. [[CrossRef](#)]
- Lin, G.R.; Pai, Y.H.; Lin, C.T.; Chen, C.C. Comparison on the electroluminescence of Si-rich SiN_x and SiO_x based light-emitting diodes. *Appl. Phys. Lett.* **2010**, *96*, 263514–263514-3. [[CrossRef](#)]
- Huang, R.; Lin, Z.; Lin, Z.; Song, C.; Wang, X.; Guo, Y.; Song, J. Suppression of Hole Overflow and Enhancement of Light Emission Efficiency in Si Quantum Dots Based Silicon Nitride Light Emitting Diodes. *IEEE J. Sel. Top. Quantum Electron.* **2013**, *20*, 212–217. [[CrossRef](#)]
- Li, N.; Wang, F.; Yang, D. Evolution of electroluminescence from silicon nitride light-emitting devices via nanostructural silver. *Nanoscale* **2013**, *5*, 3435–3440. [[CrossRef](#)] [[PubMed](#)]
- Wang, D.-C.; Hao, H.-C.; Chen, J.-R.; Zhang, C.; Zhou, J.; Sun, J.; Lu, M. White light emission and optical gains from a Si nanocrystal thin film. *Nanotechnology* **2015**, *26*, 475203. [[CrossRef](#)] [[PubMed](#)]
- Lin, Z.; Chen, K.; Zhang, P.; Xu, J.; Li, W.; Yang, H.; Huang, X. Improved power efficiency in phosphorus doped n-SiN_xO_y/p-Si heterojunction light emitting diode. *Appl. Phys. Lett.* **2017**, *110*, 081109–081109-4. [[CrossRef](#)]
- Wu, C.L.; Lin, G.R. Power Gain Modeling of Si Quantum Dots Embedded in a SiO_x Waveguide Amplifier with Inhomogeneous Broadened Spontaneous Emission. *IEEE J. Sel. Topics Quantum. Electron.* **2013**, *19*, 3000109–3000109-9.
- Negro, L.D.; Yi, J.H.; Kimerling, L.C.; Hamel, S.; Williamson, A.; Galli, G. Light emission from silicon-rich nitride nanostructures. *Appl. Phys. Lett.* **2006**, *88*, 183103. [[CrossRef](#)]
- Cen, Z.H.; Chen, T.P.; Ding, L.; Liu, Y.; Liu, Z.; Yang, M.; Wong, J.I.; Goh, W.P.; Zhu, F.R.; Fung, S. Quenching and Reactivation of Electroluminescence by Charge Trapping and Detrapping in Si-Implanted Silicon Nitride Thin Film. *IEEE Trans. Electron. Devices* **2009**, *56*, 3212–3217. [[CrossRef](#)]
- Cheng, C.H.; Wu, C.L.; Chen, C.C.; Tsai, L.H.; Lin, Y.H.; Lin, G.R. Si-rich Si_{1-x}C_{1-x} light-emitting diodes with buried Si quantum dots. *IEEE Photonics J.* **2012**, *4*, 1761–1775.
- Wang, J.; Suendo, V.; Abramov, A.; Yu, L.; Cabarrocas, P.R.I. Strongly enhanced tunable photoluminescence in polymorphous silicon carbon thin films via excitation-transfer mechanism. *Appl. Phys. Lett.* **2010**, *97*, 221113. [[CrossRef](#)]

20. Kumbhar, A.; Patil, S.B.; Kumar, S.; Lal, R.; Dusane, R.O. Photoluminescent, wide-bandgap a-SiC:H alloy films deposited by Cat-CVD using acetylene. *Thin Solid Films* **2001**, *395*, 244–248. [[CrossRef](#)]
21. Boyd, A.; Duffy, H.; McCann, R.; Cairns, M.; Meenan, B. The Influence of argon gas pressure on co-sputtered calcium phosphate thin films. *Solid Films Nucl. Instrum. Methods Phys. Res. Sect. B Beam Interact. Mater. Atoms* **2007**, *258*, 421–428. [[CrossRef](#)]
22. Svalov, A.V.; Aseguinolaza, I.R.; Garcia-Arribas, A.; Orue, I.; Barandiaran, J.M.; Alonso, J.; Fernández-Gubieda, M.L.; Kurlyand-skaya, G.V. Structure and Magnetic Properties of Thin Permalloy Films Near the “Transcritical” State. *IEEE Trans. Magn.* **2010**, *46*, 333–336. [[CrossRef](#)]
23. Khojier, K.; Savaloni, H.; Shokrai, E.; Dehghani, Z.; Dehnavi, N. Influence of argon gas flow on mechanical and electrical properties of sputtered titanium nitride thin films. *J. Theor. Appl. Phys.* **2013**, *7*, 37. [[CrossRef](#)]
24. Marwoto, P.; Fatiatun, F.; Sugianto, S.; Aryanto, D. Effects of argon pressure on the properties of ZnO:Ga thin films deposited by DC magnetron sputtering. *AIP Conf. Proc.* **2016**, *1719*, 030016–030016-6.
25. Lin, Z.; Huang, R.; Zhang, Y.; Song, J.; Li, H.; Guo, Y.; Song, C. Defect emission and optical gain in SiC_xO_y: H films. *ACS Appl. Mat. Interfaces* **2017**, *9*, 22725–22731. [[CrossRef](#)] [[PubMed](#)]
26. Inoue, Y.; Nakashima, S.; Mitsuishi, A.; Tabata, S.; Tsuboi, S. Raman spectra of amorphous SiC. *Solid State Commun.* **1983**, *48*, 1071–1075. [[CrossRef](#)]
27. Peter, S.; Bernütz, S.; Berg, S.; Richter, F. FTIR analysis of a-SiCN:H films deposited by PECVD. *Vacuum* **2013**, *98*, 81–87. [[CrossRef](#)]
28. Huang, R.; Wang, X.; Song, J.; Guo, Y.; Ding, H.; Wang, D.; Xu, J.; Chen, K. Strong orange–red light emissions from amorphous silicon nitride films grown at high pressures. *Scr. Mater.* **2010**, *62*, 643–645. [[CrossRef](#)]
29. Jha, H.S.; Yadav, A.; Singh, M.; Kumar, S.; Agarwal, P. Growth of Wide-Bandgap Nanocrystalline Silicon Carbide Films by HWCVD: Influence of Filament Temperature on Structural and Optoelectronic Properties. *J. Electron. Mater.* **2015**, *44*, 922–928. [[CrossRef](#)]
30. Huang, R.; Chen, K.; Qian, B.; Chen, S.; Li, W.; Xu, J.; Ma, Z.; Huang, X. Oxygen induced strong green light emission from low-temperature grown amorphous silicon nitride films. *Appl. Phys. Lett.* **2006**, *89*, 221120. [[CrossRef](#)]
31. Huang, R.; Lin, Z.; Guo, Y.; Song, C.; Wang, X.; Lin, H.; Xu, L.; Song, J.; Li, H. Bright red, orange-yellow and white switching photoluminescence from silicon oxynitride films with fast decay dynamics. *Opt. Mater. Express* **2014**, *4*, 205–212. [[CrossRef](#)]
32. Negro, L.D.; Yi, J.H.; Michel, J.; Kimerling, L.C.; Chang, T.-W.F.; Sukhovatkin, V.; Sargent, E.H. Light emission efficiency and dynamics in silicon-rich silicon nitride films. *Appl. Phys. Lett.* **2006**, *88*, 233109. [[CrossRef](#)]